crystals

MDPI

Article

Structural, Mechanical, Electronic, Optical, and Thermodynamic Properties of New Oxychalcogenide $A_2O_2B_2Se_3$ (A = Sr, Ba; B = Bi, Sb) Compounds: A First-Principles Study

Abdulrahman Mallah [1], Mourad Debbichi [2], Mohamed Houcine Dhaou [3,*] and Bilel Bellakhdhar [4]

1 Department of Chemistry, College of Science, Qassim University, Buraydah Almolaydah, Buraydah 51452, Saudi Arabia
2 Laboratoire de la matière condensée et nanosciences, Département de Physique, Faculté des Sciences de Monastir, Monastir 5019, Tunisia
3 Department of Physics, College of Science, Qassim University, Buraydah Almolaydah, Buraydah 51452, Saudi Arabia
4 Jeddah College of Technology, Jeddah 21361, Saudi Arabia
* Correspondence: m.dhaou@qu.edu.sa

Abstract: The structural, mechanical, electronic, and optical characteristics of Alkali chalcogenide and oxychalcogenides, i.e., $A_2O_2B_2Se_3$ (A = Sr, Ba; B = Bi, Sb), were investigated using density functional theory (DFT). After full relaxation, the obtained structural parameters are in good agreement with the experimental parameters. Furthermore, the calculated elastic stiffness C_{ij} shows that all of the studied compounds followed the mechanical stability criteria. Ductility for these compounds was analyzed by calculating Pugh's ratio; we classified the $Sr_2O_2Bi_2Se_3$, $Sr_2O_2Sb_2Se_3$, and $Ba_2O_2Bi_2Se_3$ as ductile, and the $Ba_2O_2Sb_2Se_3$ as brittle. The Debye temperature and acoustic velocity were estimated. In addition, electronic and chemical bonding properties were studied from the analysis of the band structure and density of state. The main features of the valence and conduction bands were analyzed from the partial density of states. Electronic band structures are mainly contributed to by Se-4*p* and Bi-6*p*/Sb-5*p* states. Direct band gaps are 0.90, 0.47, and 0.73 eV for $Sr_2O_2Bi_2Se_3$, $Sr_2O_2Sb_2Se_3$, and $Ba_2O_2Sb_2Se_3$, respectively. The $Ba_2O_2Bi_2Se_3$ compound has an indirect band gap of 1.12 eV. Furthermore, we interpreted and quantified the optical properties, including the dielectric function, absorption coefficient, optical reflectivity, and refractive index. From the reflectivity spectra, we can state that these compounds will be useful for optical applications.

Keywords: DFT; alkali chalcogenide; mechanical property; ab initio calculations; oxychalcogenide

Citation: Mallah, A.; Debbichi, M.; Dhaou, M.H.; Bellakhdhar, B. Structural, Mechanical, Electronic, Optical, and Thermodynamic Properties of New Oxychalcogenide $A_2O_2B_2Se_3$ (A = Sr, Ba; B = Bi, Sb) Compounds: A First-Principles Study. *Crystals* **2023**, *13*, 122. https://doi.org/10.3390/cryst13010122

Academic Editor: Sergio Brutti

Received: 12 December 2022
Revised: 24 December 2022
Accepted: 28 December 2022
Published: 10 January 2023

1. Introduction

Materials based on transition metal ions have attracted a lot of attention due to their unusual electrical, magnetic, and structural features [1,2]. Mixed-anion compounds containing oxide and chalcogenide anions have been extensively studied since the discovery of superconductivity in F-doped LaOFeAs at critical temperatures T∼26 K [3]. This result has accelerated studies on new layered materials. One of the most important compounds, layered oxychalcogenides, are mixed-anion compounds; chalcogenide and oxide anions are indirectly bounded via one or more cations, creating a stack of alternating oxide and chalcogenide layers [4,5].

The oxychalcogenides have attracted much interest owing to their rich and diverse chemistry, and are characterized by the coexistence of ionic oxide anions and more covalent chalcogenide anions. For example, oxide chalcogenides with the chemical formula $A_2MO_2X_2Ch_2$ (where A = Sr, Ba; X = Cu, Ag; Ch = S, Se and M = first-row transition metal) were first reported by Zhu et al. [6,7] and are isostructural with $Sr_2Mn_3Sb_2O_2$ structure. It

was also found that it is possible to synthesize compounds with different thicknesses of the oxides and chalcogenide layers by varying the element ratios and heating conditions [8].

Currently, the most explored of such materials are bismuth chalcogenide compounds, particularly $BiCh_2$ (Ch = S, Se)-based compounds; many of them possess layered or tunneled structures. Bi_2O_2Ch (Ch = S, Se) have been exploited for their photocatalytic activities and thermoelectric properties [9,10]. The quaternary oxychalcogenides with 1111 stoichiometry BiMOCh (Ch = S, Se; M = Cu, Ag), due to their outstanding mechanical, chemical, electrical, and optical properties, have gained extensive attention as ionic and transparent conductors. The BiS_2-based superconductive compounds $YO_{1-x}F_xBiS_2$ (Y = La, Nd, Pr, and Ce), with the highest Tc of 10 K, have then been discovered and $NdO_{1-x}F_xBiS_2$ (x = 0.1–0.7) was found to have a maximum Tc of less than 5.6 K [11].

One such development is the discovery of new superconductivity compounds that exhibit zero resistance below a critical temperature (Tc). This progress requires the synthesis of new products with novel and fascinating properties. Recently, alkali chalcogenide and oxychalcogenides, i.e., $A_2O_2B_2Se_3$ (A = Sr, Ba; B = Bi, Sb) materials were synthesized by direct combination of SrO or BaO with Bi_2Se_3 or Sb_2Se_3 [12]. Insulating behavior has been revealed for all compounds. The crystal structure and chemical composition of these compounds were determined by X-ray powder diffraction (XRPD). Their structures consist of electronically active quasi-one-dimensional Sb-Se or Bi-Se ribbons isolated from one another by SrO units. Moreover, the structures of $A_2O_2B_2Se_3$ compounds share structural features with numerous bismuth and antimony chalcogenides, such as the ternary AB_2X_4 (A = Sr, Ba; B = Bi, Sb; X = S, Se). Since their structural and electronic similarity with the $LnOBiX_2$ (X = S, Se and Ln = La, Nd, Ce, Pr, Yb) superconductors [11,12], this new family provides a one-of-a-kind opportunity to consider the impacts of dimensionality on superconductivity.

The modeling of physical properties (by means of DFT techniques) has become a very useful tool for understanding the structural, electronic, mechanical, optical, and thermodynamic properties of various materials. In the present work, we would make a theoretical study of the electronic structure, elastic and optical properties of $A_2O_2B_2Se_3$ (A = Sr, Ba and B = Bi, Sb) materials using first-principle calculations. In Section 2, we provide the computational details of the calculations. Our results are presented in Section 3. A summary of the results is provided in Section 4.

2. Computational Methodology

The first-principles calculations were performed with the Quantum espresso code [13] using the generalized gradient approximation (GGA) in the form of Perdew–Burke–Ernzerhof (PBE) [14] to describe the exchange–correlation functional (XC). The plane waves of the electronic wave functions were expanded on the basis of a plane wave set with an energy cut-off of 40 Ry. the irreducible Brillouin zone was integrated with Monkhorst–Pack [15] $4 \times 4 \times 4$ *k*-point mesh. For the density of state (DOS) calculations, we used a mesh of $12 \times 12 \times 12$ with the tetrahedron method integration in order to obtain the high-quality charge density. An ultrasoft pseudo-potential [16] was adopted to describe the ionic cores and the valance electron interactions. In order to improve the convergence of the solution of the self-consistent Kohn–Sham equations, the energy levels were broadened by the Methfessel–Paxton [17] smearing with a Gaussian spreading $\sigma = 0.01$ Ry. The total energy convergence in the iterative solution of the Kohn–Sham equations [18] was set at 1.0×10^{-7} Ry to obtain well-converged ground state energy. All structures were fully relaxed by using the BFGS algorithm [19] with a threshold force of 10^{-3} Ry/Bohr.

3. Results and Discussion

3.1. Crystal Structure

$A_2O_2B_2Se_3$ (A = Sr, Ba; B = Bi, Sb) materials crystallized in monoclinic structures with the $P2_1C$ (No. 14) space group as displayed in Figure 1. The structures of these materials are described in detail by Jessica et al. [12], consisting of double-chain–quasi-one-dimensional

ribbons of edge-linked BSe_4O square pyramids, connected to SrO fragments by the apical B-O bond.

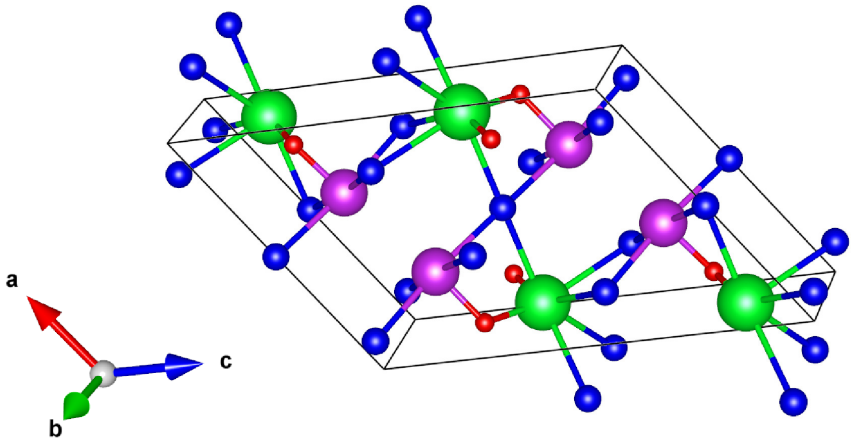

Figure 1. Crystal structure of the $A_2O_2B_2Se_3$ (A = Sr, Ba, and B = Bi, Sb) compounds, space group $P2_1/c$ (No. 14). Green, violet, red, and blue represent A, B, O, and Se atoms.

Table 1 summarizes our calculated structural parameters (a, b, c, and angle β) and the formation energies for all compounds compared with the available experimental data. It appears from our results that optimized equilibrium parameters for $Sr_2O_2Bi_2Se_3$, $Sr_2O_2Sb_2Se_3$, and $Ba_2O_2Bi_2Se_3$ agree well with the experimental values reported in Reference [12]. For $Ba_2O_2Sb_2Se_3$, there are no corresponding experimental data for the lattice parameters. Moreover, by examining the structural parameters, the substitution of Sr by Ba and Sb by Bi tends to increase the lattice parameters, which may be interpreted in terms of the larger ionic radii of Ba^{2+}(0.134 Å) and Bi^{3+}(0.96 Å) compared to that of Sr^{2+}(1.12 Å) and Sb^{3+}(0.76 Å).

The relative stability of the $A_2O_2B_2Se_3$ (A = Sr, Ba; B = Bi, Sb) materials was examined by calculating their formation energies, E_{form}, defined as:

$$E_{form} = \frac{E(A_2O_2B_2Se_3) - 2E(A) - 2 \times \frac{1}{2}E(O_2) - 2E(B) - 3E(Se)}{9} \quad (1)$$

where $E(A_2O_2B_2Se_3)$ is the total energy of one unit cell of the $A_2O_2B_2Se_3$ compound. E(A), E(B), and E(Se) are the energies of each atom for A, B, and Se in their stable bulk phases, respectively. $E(O_2)$ is the total energy per O_2 molecule.

The calculated formation energies of the different compounds are regrouped in Table 1. As seen, the calculated values are all negatives, confirming the relative stability of all compounds.

Table 1. Calculated lattice parameters a, b, c (Å), β (°), formation energy, E_{form} (eV) of the studied $A_2O_2B_2Se_3$ (A = Sr, Ba and B = Bi, Sb) materials compared with the available experimental data from Reference [12]. $\alpha = \gamma = 90°$.

	$Sr_2O_2Bi_2Se_3$	$Sr_2O_2Sb_2Se_3$	$Ba_2O_2Bi_2Se_3$	$Ba_2O_2Sb_2Se_3$
$a_{calc.}$	9.200	9.199	9.463	9.729
$a_{exp.}$	9.499	9.424	9.820	-
$b_{calc.}$	4.005	3.957	4.095	4.122
$b_{exp.}$	4.084	4.057	4.190	-
$c_{calc.}$	13.111	12.987	13.535	13.723
$c_{exp.}$	13.437	13.341	13.904	-
$\beta_{calc.}$	122.828	123.000	123.298	124.040
$\beta_{exp.}$	122.861	121.955	123.692	-
E_{form}	−2.145	−2.173	−2.139	−2.147

3.2. Mechanical Properties

The mechanical properties of these compounds are important for their potential technological and industrial applications. Elastic constants, needed to determine the mechanical stability of these compounds, were calculated. They give an overview of the mechanical and dynamical characteristics, especially the stability and stiffness of the present materials.

For monoclinic crystal [20,21], 13 independent elastic constants, i.e., C_{11}, $C_{12} = C_{21}$, C_{22}, $C_{13} = C_{31}$, $C_{23} = C_{32}$, C_{33}, C_{44}, $C_{15} = C_{51}$, $C_{25} = C_{52}$, $C_{35} = C_{53}$, C_{55}, $C_{46} = C_{64}$, and C_{66} remained with the explicit form of the tensor reduced to:

$$\begin{pmatrix} C_{11} & C_{12} & C_{13} & 0 & C_{15} & 0 \\ C_{12} & C_{22} & C_{23} & 0 & C_{25} & 0 \\ C_{13} & C_{23} & C_{33} & 0 & C_{35} & 0 \\ 0 & 0 & 0 & C_{44} & 0 & C_{46} \\ C_{15} & C_{25} & C_{35} & 0 & C_{55} & 0 \\ 0 & 0 & 0 & C_{46} & 0 & C_{66} \end{pmatrix}$$

In Table 2, we present the calculated thirteen independent elastic constants C_{ij} for the monoclinic lattice structures.

Table 2. The calculated elastic constants of the $A_2O_2B_2Se_3$ (A = Sr, Ba and B = Bi, Sb) compounds in the units of GPa.

	$Sr_2O_2Bi_2Se_3$	$Sr_2O_2Sb_2Se_3$	$Ba_2O_2Bi_2Se_3$	$Ba_2O_2Sb_2Se_3$
C_{11}	106.86	107.04	102.65	54.30
C_{22}	133.74	137.47	125.26	108.80
C_{33}	122.92	126.51	118.39	109.62
C_{44}	39.56	35.86	51.37	43.83
C_{55}	32.48	34.53	31.00	29.42
C_{66}	26.02	28.87	26.00	28.07
C_{12}	31.42	31.87	32.16	22.79
C_{13}	35.93	36.20	35.23	26.23
C_{23}	56.48	55.99	57.86	46.94
C_{15}	5.37	4.85	6.93	4.14
C_{25}	2.10	1.05	5.57	11.66
C_{35}	10.66	12.69	6.35	9.04
C_{46}	0.48	2.40	2.10	3.14

It is known that, for the monoclinic structure, mechanical stability requires elastic constants satisfying the following Born's criteria [22]:

$C_{ii} > 0\,(i = 1, 6)$, $(C_{11} + C_{22} + C_{33} + 2(C_{12} + C_{13} + C_{23})) > 0$, $(C_{33}C_{55} - C_{35}^2) > 0$, $(C_{44}C_{66} - C_{46}^2) > 0$,

$(C_{22} + C_{33} - 2C_{23}) > 0$, $[C_{22}(C_{33}C_{55} - C_{35}^2) + 2C_{23}C_{25}C_{35} - C_{23}^2C_{55} - C_{25}^2C_{33}] > 0$,

and

$$\{2[C_{15}C_{25}(C_{33}C_{12} - C_{13}C_{23}) + C_{15}C_{35}(C_{22}C_{13} + C_{12}C_{23}) + C_{25}C_{35}(C_{11}C_{23} - C_{12}C_{13})] - [C_{15}^2(C_{22}C_{33} - C_{23}^2) + C_{25}^2(C_{11}C_{33} - C_{13}^2) + C_{35}^2(C_{11}C_{22} - C_{12}^2)] + gC_{55}\} > 0,$$

where $g = C_{11}C_{22}C_{33} - C_{11}C_{23}^2 - C_{22}C_{13}^2 - C_{33}C_{12}^2 + 2C_{12}C_{13}C_{23}$. Therefore, these four compounds are structurally and mechanically stable.

The macroscopic mechanical properties of the different crystals, namely Young's modulus, bulk modulus, Poisson's ratio, and shear modulus, can be determined by the obtained elastic constants using the equations presented in Reference [23].

The bulk modulus (B) expresses the response of a material to a volume change of the hydrostatic pressure, whereas the shear modulus (G) reflects the resistance of a material to a shape change, and is deduced from elastic and compliance constants. Voigt [24] proposed to

express the polycrystalline bulk modulus B_V and shear modulus G_V via the combinations of elastic constants C_{ij}. Similarly, Reuss and Angew [25] determined the bulk modulus B_R and shear modulus G_R expressions in terms of compliance constants S_{ij}. Moreover, Hill [26] calculated B and G from the average of the Voigt and Reuss bounds as:

$$B = \frac{B_V + B_R}{2}, G = \frac{G_V + G_R}{2}.$$

The polycrystalline Young's modulus (E) and Poisson's ratio (ν) are calculated using the relationships [26]

$$E = \frac{9BG}{3B + G}, \nu = \frac{3B - 2G}{6B + 2G}.$$

The values of these polycrystalline elastic constants are listed in Table 3. We can see from this table that all compounds exhibit good mechanical properties. The $Sr_2O_2Sb_2Se_3$ compound has larger bulk and shear modulus, indicating that it presents better mechanical properties compared to the others, which mainly attributes to the more stable Sr-O-Sb bond than Sr-O-Bi, Ba-O-Bi, and Ba-O-Sb. As also seen, the bulk modulus B is larger than the shear modulus G for all compounds, implying that G limits their stabilities.

Accordingly, we calculate "Pugh's criterion" ($D = B/G$), which is proposed to judge a metal's ductility and brittleness; the critical value that separates brittle and ductile materials is around 1.75 [27]. As shown in Table 3, Pugh's ratio is $D > 1.75$ for $Sr_2O_2Bi_2Se_3$, $Sr_2O_2Sb_2Se_3$, and $Ba_2O_2Bi_2Se_3$; thus, they behave in a ductile manner. The calculated D ratio for $Ba_2O_2Sb_2Se_3$ is less than 1.75, so it exhibits brittle behavior.

Table 3. The calculated polycrystalline elastic constants (B (GPa), G (GPa), and E (GPa)), and Poisson's ratio ν and Pugh's ratio (D) for $A_2O_2B_2Se_3$ (A = Sr, Ba and B = Bi, Sb) materials.

	B	***G***	***E***	***ν***	***D***	**Type**
$Sr_2O_2Bi_2Se_3$	66.523	34.755	88.801	0.277	1.914	ductile
$Sr_2O_2Sb_2Se_3$	67.333	35.566	90.723	0.275	1.893	ductile
$Ba_2O_2Bi_2Se_3$	64.817	35.201	89.417	0.270	1.841	ductile
$Ba_2O_2Sb_2Se_3$	46.913	30.764	75.737	0.230	1.525	brittle

3.3. Electronic Structure

Band structure calculations are required to provide more information for the fabrication and development of electronic and optoelectronic devices. To explore the electronic properties of the $A_2O_2B_2Se_3$ compounds, the energy band structures and the partial density of states (PDOS) of the four compounds are illustrated in Figure 2.

One can notice that band structures show similar shapes but with different gap values. It can be clearly seen that $Sr_2O_2Bi_2Se_3$, $Sr_2O_2Sb_2Se_3$, and $Ba_2O_2Sb_2Se_3$ show direct band gaps of 0.90, 0.47, and 0.73 eV, respectively, with the valence band maximum (VBM) and the conduction band minimum (CBM) lying at the Γ point. However, $Ba_2O_2Bi_2Se_3$ has an indirect band gap of 1.12 eV where the VBM is at the Γ point and the CBM is at the Y point. The difference between the experimental value and the theoretical one can be attributed to some aspects, such as the experimental environment and the exchange–correlation description considered in the present study.

From the partial density of states (PDOS), it can be observed that the VBMs of all compounds mainly consist of Se-4p states, while the CBM is composed of Bi-6p/Sb-5p states. We can see the contribution of the A states at the lowest-lying states. A strong hybridization between Sb and Se states was observed in the conduction band for the $Ba_2O_2Sb_2Se_3$ compound.

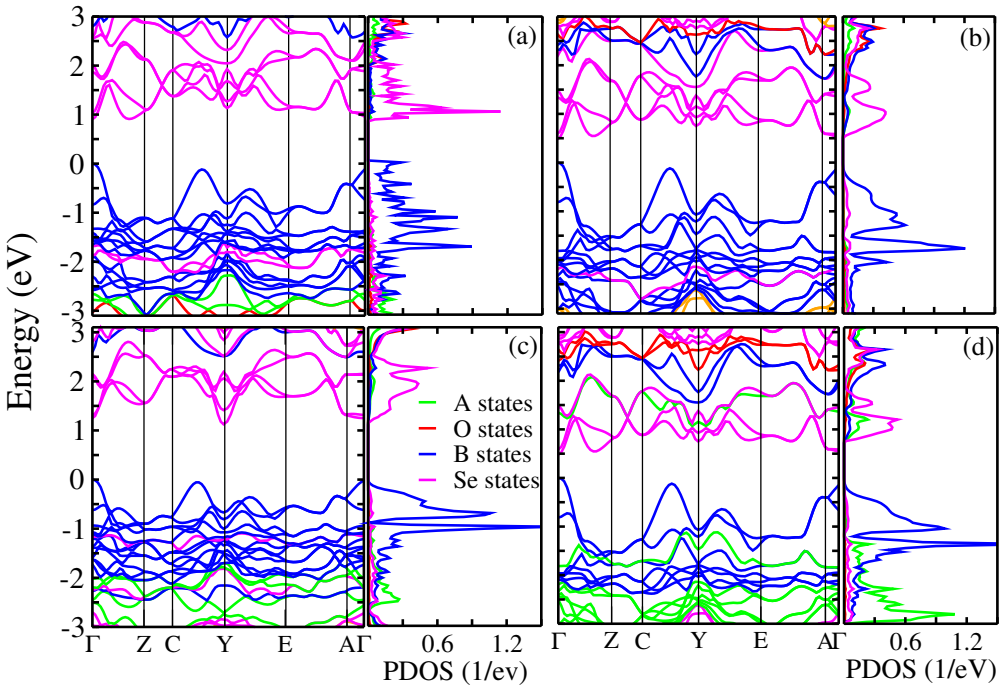

Figure 2. (color online) Calculated band structures and partial density of states for (**a**) $Sr_2O_2Bi_2Se_3$, (**b**) $Sr_2O_2Sb_2Se_3$, (**c**) $Ba_2O_2Bi_2Se_3$, and (**d**) $Ba_2O_2Sb_2Se_3$. A refers to Sr or Ba and B replaces Bi or Sb.

3.4. Optical Properties

Optical response functions of the materials are described by the complex dielectric function ($\varepsilon(\omega) = \varepsilon_1(\omega) + i\varepsilon_2(\omega)$). It gives the optical response of the medium at all photon energies $E = \hbar\omega$ and it is closely related to the electronic structure of the material. The imaginary part of the dielectric function $\varepsilon_2(\omega)$ is calculated using the matrix elements of occupied and unoccupied wave functions; it is given as follows [28]:

$$\varepsilon_2(\omega) = \frac{Ve^2}{2\pi m^2\hbar^2\omega^2}\int d^3k \sum_{n,n'} |< kn|p|kn' >|^2 f(kn) \times (1 - f(kn'))\delta(E_{kn} - E_{kn'} - \hbar\omega),$$

where n and n' are the initial and final states, respectively, p is the momentum operator $(\hbar/i)\partial/\partial x$, $|kn>$ is a crystal wave function, $f(kn)$ is the Fermi function for the n^{th} state, and $\hbar\omega$ is the energy of the incident photon. The real part $\varepsilon_1(\omega)$ of the dielectric function can be obtained from the imaginary part $\varepsilon_2(\omega)$ through the Kramers–Kroning relations [29,30],

$$\varepsilon_1(\omega) = 1 + \frac{2}{\pi}P\int_0^\infty \frac{\omega'\varepsilon_2(\omega')}{\omega'^2 - \omega^2}d\omega'.$$

P implies the principal value of the integral.

The optical reflectivity spectra $R(\omega)$, the refractive index $n(\omega)$, and the absorption coefficient $\alpha(\omega)$ are derived from the dielectric function as follows [30–32]:

$$R(\omega) = \left|\frac{\sqrt{\varepsilon(\omega)} - 1}{\sqrt{\varepsilon(\omega)} + 1}\right|^2,$$

$$n(\omega) = \left[\frac{\varepsilon_1(\omega) + (\varepsilon_1^2(\omega) + \varepsilon_2^2(\omega))^{1/2}}{2}\right]^{1/2}$$

and

$$\alpha(\omega) = \left[2\omega^2\left(\sqrt{\varepsilon_1^2(\omega) + \varepsilon_2^2(\omega)} - \varepsilon_2(\omega)\right)\right]^{1/2}$$

We note that this part of the Brillouin zone integration was performed using the tetrahedron method with denser *k*-points in the irreducible part of the Brillouin zone without broadening. Moreover, all the calculations are along parallel and perpendicular directions to the directions of propagation.

Since the dielectric function and the absorption coefficient play crucial roles in the characterization and optical applications of materials, we discuss the optical properties of the $A_2O_2B_2Se_3$ (A = Sr, Ba; B = Bi, Sb) in this section.

The calculated imaginary part shows three different components of dielectrics, which predict the anisotropic nature of the materials. In Figure 3a, we present only imaginary part of the dielectric function for E||a. The peaks were caused by transitions from the upper valence band to the lower conduction band. These correspond to transitions from Se-4*p* valence states to Bi-6*p*/Sb-5*p* conduction band. It is noted that the ε_2 of all studied materials have similar shapes but different amplitudes because of the similar band structures. Moreover, the ε_2 of $Sr_2O_2Bi_2Se_3$ and $Ba_2O_2Bi_2Se_3$ were much higher than that of the $Sr_2O_2Sb_2Se_3$ and $Ba_2O_2Sb_2Se_3$, showing remarkably enhanced absorption of the photons.

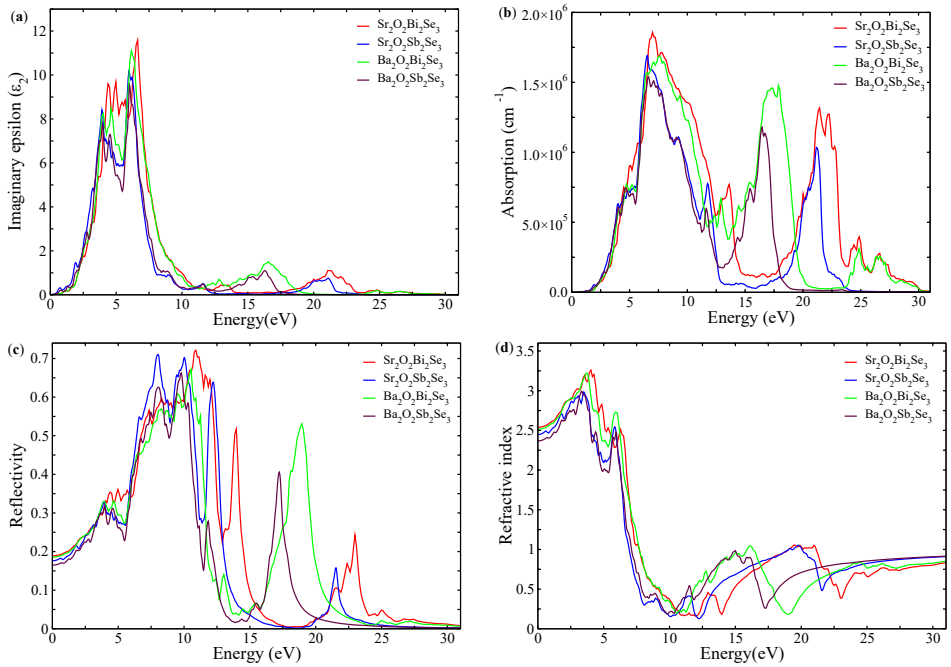

Figure 3. Optical spectrum of $A_2O_2B_2Se_3$ (A = Sr, Ba; B = Bi, Sb) compounds for E||a. (**a**) Imaginary part of the dielectric function, (**b**) absorption coefficient, (**c**) reflection spectra, and (**d**) refractive index.

The absorption coefficient defines the region where a material absorbs energy. The energy dependence of the absorption spectrum of the present compounds for E||a is given in Figure 3b. The absorption edge is away from 0 eV, which corresponds to the energy gaps. The absorption coefficient exhibits two prominent peaks indicating that they could absorb visible light. The first peaks of $Sr_2O_2Bi_2Se_3$ and $Ba_2O_2Bi_2Se_3$ are present in the same region at around 3 eV and extend to 12 eV, the second peaks are located at 16 eV and 24 eV for $Ba_2O_2Bi_2Se_3$ and $Sr_2O_2Bi_2Se_3$, respectively. For $Sr_2O_2Sb_2Se_3$ and $Ba_2O_2Sb_2Se_3$, the same trend is found but in a different region of adsorption. Notably, they exhibited two prominent peaks.

The reflection spectra of the studied compounds are presented in Figure 3c. We can see that the spectra are mainly in the areas between 5 eV and 25 eV, after that, the reflectivity falls sharply to low values (high transparency) for higher energy ranges. The peaks of the reflectivity correspond to the dielectric peaks, which is the macroscopic expression of the inter-band transition behavior. Several obvious peaks are identified, which correspond to

the transition from the valence bands to the conduction bands located at 7, 10, 11, 14, 15, 18, 21, and 24 eV.

The calculated refractive index of the studied materials is shown in Figure 3d. The refractive index spectra of all studied materials show similar features, first reaching a maximum value of around 3.3 at around 4 eV, falling at intermediate energies, and then the curve vanishes at higher energies. Indeed, beyond certain energy, the considered material absorbs high-energy photons and cannot behave as transparent material. The extracted static refractive indices are 2.51, 2.48, 2.50, and 2.47 for $Sr_2O_2Bi_2Se_3$, $Ba_2O_2Bi_2Se_3$, $Sr_2O_2Sb_2Se_3$, and $Ba_2O_2Sb_2Se_3$, respectively.

3.5. Thermodynamic Properties

Thermodynamic properties of materials, such as specific heat, melting temperature, and thermal conductivity [33] are most suitably described in terms of the Debye temperature (θ_D). It is a fundamental and very important parameter that helps to obtain the thermodynamic properties and stability of crystals and, thus, design and develop new materials. At a low temperature, the average sound velocities (v_m) and the Debye temperature (θ) can be calculated from elastic constants taking into account the fact that the vibrational excitations arise solely from acoustic vibrations. We calculated the θ_D from the average sound velocity through the following equation v_m [34]:

$$\theta_D = \frac{h}{k_B}\left[\frac{3n}{4\pi V_a}\right]^{1/3},$$

where h is Planck's constant, k_B is Boltzmann's constant, V_a is the atomic volume, n is the number of atoms per formula unit, and v_m can be obtained from [34]:

$$v_m = \left[\frac{1}{3}\left(\frac{2}{v_t^3} + \frac{1}{v_l^3}\right)\right]^{-1/3},$$

where v_t is transverse velocity, v_l is longitudinal velocity. v_t and v_l are calculated from Navier's equation [35]:

$$v_t = \left[\frac{4G + 3B}{3\rho}\right]^{1/2} \text{ and } v_l = \left[\frac{G}{\rho}\right]^{1/2}.$$

The calculated results of Debye temperatures, transverse, longitudinal, and average sound velocities are given in Table 4. $Sr_2O_2Sb_2Se_3$ has a higher Debye temperature; thus, it has a greater micro-hardness. According to References [36–38], a larger θ suggests a higher normal vibration, which is associated with better thermal conductivity. Meanwhile, the Debye temperature can characterize the strength of the covalent bond for the solid. Unfortunately, to the best of our knowledge, there are no other theoretical or measured data available in the literature to compare with our results. Nevertheless, we hope that our results can support further experiments.

Table 4. Calculated Debye temperature θ_D (K), average elastic wave velocities v_m (ms^{-1}), longitudinal v_l (ms^{-1}), and transverse v_t (ms^{-1}) for $A_2O_2B_2Se_3$ (A = Sr, Ba, and B = Bi, Sb) compounds.

	θ_D	v_l	v_t	v_m
$Sr_2O_2Bi_2Se_3$	260.55	4000.36	2219.89	2472.64
$Sr_2O_2Sb_2Se_3$	293.61	4463.99	2482.98	2765.16
$Ba_2O_2Bi_2Se_3$	250.38	3918.86	2189.84	2437.81
$Ba_2O_2Sb_2Se_3$	255.84	3833.41	2245.95	2490.15

4. Conclusions

In summary, first-principles calculations were performed on the $A_2O_2B_2Se_3$ (A = Sr, Ba; B = Bi, Sb) compounds, including structural parameters, band structure, the density of state, elastic constants, and optical parameters. Our study shows that all studied materials are mechanically stable. By analyzing the band structures and the DOS, we show that the $Sr_2O_2Bi_2Se_3$, $Sr_2O_2Sb_2Se_3$, and $Ba_2O_2Sb_2Se_3$ compounds have direct band gaps while $Ba_2O_2Bi_2Se_3$ possesses an indirect band gap. In addition, this paper also shows that the $Sr_2O_2Bi_2Se_3$, $Sr_2O_2Sb_2Se_3$, and $Ba_2O_2Bi_2Se_3$ are ductile while $Ba_2O_2Sb_2Se_3$ is brittle. Moreover, the calculated refractive indices n(0) for all compounds are in the range of 2.47–2.51, making them good candidates for use as waveguides. Finally, this new family offers a unique chance to research the impact of dimensionality on superconductivity due to the structural and electronic similarities between them and the $LnOBiX_2$ (X = S, Se, and Ln = La, Nd, Ce, Pr, Yb) superconductors.

Author Contributions: Conceptualization: A.M., M.D., M.H.D. and B.B.; data curation: A.M., M.D. and M.H.D.; formal analysis: M.D., M.H.D. and B.B.; Investigation: A.M., M.D. and M.H.D.; resources: M.D.; validation: A.M. and M.D.; writing—original draft: A.M., M.D. and M.H.D. All authors have read and agreed to the published version of the manuscript.

Funding: Qassim University, represented by the Deanship of Scientific Research, on the material support for this research under the number (10244-cos-2020-1-3-I).

Data Availability Statement: Data can be requested from the authors.

Acknowledgments: The authors gratefully acknowledge Qassim University, represented by the Deanship of Scientific Research, on the material support for this research under the number (10244-cos-2020-1-3-I) during the academic year 1442AH/2020AD.

Conflicts of Interest: The authors declare no conflict of interest.

References

1. Chen, H.; McClain, R.; Shen, J.; He, J.; Malliakas, C.D.; Spanopoulos, I.; Zhang, C.; Zhao, C.; Wang, Y.; Li, Q.; et al. Christopher Wolverton, and Mercouri G. Kanatzidis. *Inorg. Chem.* **2022**, *61*, 8240.
2. Njema, H.; Debbichi, M.; Boughzala, K.; Said, M.; Bouzouita, K. Structural, electronic and thermodynamic properties of britholites $Ca_{10-x}Lax\ (PO4)_{6-x}(SiO4)_xF_2(0 \leq x \geq 6)$: Experiment and theory *Mater. Res. Bull.* **2014**, *51*, 216. [CrossRef]
3. Kamihara, Y.; Watanabe, T.; Hirano, M.; Hosono, H. Iron-Based Layered Superconductor $La[O_{1-x}F_x]FeAs$ (x = 0.05–0.12) with T_c = 26 K.*J. Am. Chem. Soc.* **2008**, *130*, 3296–3297. [CrossRef] [PubMed]
4. Zagorac, D.; Doll, K.; Zagorac, J.; Jordanov, D.; Matović, B. Barium sulfide under pressure: discovery of metastable polymorphs and investigation of electronic properties on ab initio level. *Inorg. Chem.* **2017**, *56*, 10644–10654. [CrossRef]
5. Wang, R.; Zhao, Y.; Zhang, X.; Huang, F. Structural dimension modulation in a new oxysulfide system of $Ae_2Sb_2O_2S_3$ (Ae = Ca and Ba). *Inorg. Chem. Front.*, **2022**, *9*, 3552–3558. [CrossRef]
6. Zhu, W.J.; Hor, P.H.; Jacobson, A.J.; Crisci, G.; Albright, T.A.; Wang, S.-H.; Vogt, T. $A_2Cu_2CoO_2S_2$ (A= Sr, Ba), a novel example of a square-planar CoO_2 layer. *J. Am. Chem. Soc.* **1997**, *119*, 12398–12399. [CrossRef]
7. Zhu, W.J.; Hor, P.H. Unusual layered transition-metal oxysulfides: $Sr_2Cu_2MO_2S_2$ (M = Mn, Zn). *J. Solid State Chem.* **1997**, *130*, 319–321. [CrossRef]
8. Zhao, J.; Islam, S.M.; Kontsevoi, O.Y.; Tan, G.; Stoumpos, C.C.; Chen, H.; Li, R.K.; Kanatzidis, M.G. The Two-Dimensional $A_xCd_xBi_{4-x}Q_6$ (A = K, Rb, Cs; Q = S, Se): Direct Bandgap Semiconductors and Ion-Exchange Materials. *J. Am. Chem. Soc.* **2017**, *139*, 6978–6987. [CrossRef]
9. Pacquette, A.L.; Hagiwara, H.; Ishihara, T.; Gewirth, A.A. Fabrication of an oxysulfide of bismuth Bi_2O_2S and its photocatalytic activity in a Bi_2O_2S/In_2O_3 composite. *J. Photochem. Photobiol. A* **2014**, *277*, 27–36. [CrossRef]
10. Ruleova, P.; Drasar, C.; Lostak, P.; Li, C.-P.; Ballikaya, S.; Uher, C. Thermoelectric properties of Bi_2O_2Se. *Mater. Chem. Phys.* **2010**, *119*, 299–302. [CrossRef]
11. Yazici, D.; Huang, K.; White, B.D.; Chang, A.H.; Friedman, A.J.; Maple, M.B. Superconductivity of F-substituted Ln $OBiS_2$ (Ln = La, Ce, Pr, Nd, Yb) compounds. *Philos. Mag.* **2013**, *93*, 673–680. [CrossRef]
12. Panella, J.R.; Chamorro, J.; McQueen, T.M. Synthesis and Structure of Three New Oxychalcogenides: $A_2O_2Bi_2Se_3$ (A = Sr, Ba) and $Sr_2O_2Sb_2Se_3$. *Chem. Mater.* **2016**, *28*, 890–895. [CrossRef]
13. Giannozzi, P.; Baroni, S.; Bonini, N.; Calandra, M.; Car, R.; Cavazzoni, C.; Ceresoli, D.; Chiarotti, G.L.; Cococcioni, M.; Dabo, I.; et al. QUANTUM ESPRESSO: A modular and open-source software project for quantum simulations of materials. *J. Phys. Condens. Mat.* **2009**, *21*, 395502. [CrossRef]

14. Perdew, J.P.; Burke, K.; Ernzerhof, M. Generalized gradient approximation made simple. *Phys. Rev. Lett.* **1996**, *77*, 3865. [CrossRef]
15. Wisesa, P.; McGill, K.A.; Mueller, T. Efficient generation of generalized Monkhorst-Pack grids through the use of informatics. *Phys. Rev. B* **2016**, *93*, 155109. [CrossRef]
16. Yates, J.R.; Pickard, C.J.; Mauri, F. Calculation of NMR chemical shifts for extended systems using ultrasoft pseudopotentials. *Phys. Rev. B* **2007**, *76*, 024401. [CrossRef]
17. Methfessel, M.; Paxton, A.T. High-precision sampling for Brillouin-zone integration in metals. *Phys. Rev. B* **1989**, *40*, 3616. [CrossRef]
18. Baerends, E.J. Perspective on "Self-consistent equations including exchange and correlation effects". *Theor. Chem. Acc.* **2000**, *103*, 265–269. [CrossRef]
19. Mokhtari, A.; Ribeiro, A. Global Convergence of Online Limited Memory BFGS. *J. Mach. Learn. Res.* **2015**, *16*, 3151–3181.
20. Iuga, M.; Neumann, G.S.; Meinhardt, J. Ab-initio simulation of elastic constants for some ceramic materials. *Eur. Phys. J. B* **2007**, *58*, 127–133. [CrossRef]
21. Golesorkhtabar, R.; Pavone, P.; Spitaler, J.; Puschnig, P.; Draxl, C. ElaStic: A tool for calculating second-order elastic constants from first principles. *Comp. Phys. Commun.* **2013**, *184*, 1861–1873. [CrossRef]
22. Nye, J.F. *Physical Properties of Crystals*; Oxford University Press: New York, NY, USA, 1985.
23. Debbichi, M.; Alresheedi, F. First-principles calculations of mechanical, electronic and optical properties of a new imidooxonitridophosphate. *Chem. Phys.* **2020**, *538*, 110917. [CrossRef]
24. Voigt, W. *Lehrburch der Kristallphys*; Teubner Press: Leipzig, Germany, 1928.
25. Reuss, A. Berechnung der Fließgrenze von Mischkristallen auf Grund der Plastizitätsbedingung für Einkristalle. *Z. angew. Math. Mech.* **1929**, *9*, 49–58. [CrossRef]
26. Hill, R. The elastic behaviour of a crystalline aggregate. *Proc. Phys. Soc. Lond.* **1952**, *65*, 349.
27. Pugh, S.F. XCII. Relations between the elastic moduli and the plastic properties of polycrystalline pure metals. *Lond. Edinb. Dublin Philosoph. Mag. J. Sci.* **1954**, *45*, 823–843. [CrossRef]
28. Saha, S.; Sinha, T.P.; Mookerjee, A. Electronic structure, chemical bonding, and optical properties of paraelectric $BaTiO_3$. *Phys. Rev. B* **2000**, *62*, 8828. [CrossRef]
29. Wooten, F. *Optical Properties of Solids*; Academic: New York, NY, USA, 1972.
30. Yu, Y.P.; Cardona, M. *Fundamentals of Semiconductors: Physics and Materials Properties*, 2nd ed.; Springer: Berlin/Heidelberg, Germany, 1999.
31. Ravindran, P.; Delin, A.; James, P.; Johansson, B.; Wills, J.M.; Ahuja, R.; Eriksson, O. Magnetic, optical, and magneto-optical properties of MnX (X = As, Sb, or Bi) from full-potential calculations. *Phys. Rev. B* **1999**, *59*, 15680. [CrossRef]
32. Fox, M. *Optical Properties of Solids*; Oxford University Press: New York, NY, USA, 2001.
33. Fan, Q.Y.; Wei, Q.; Yan, H.Y.; Zhang, M.G.; Zhang, Z.X.; Zhang, J.Q. Elastic and electronic properties of Pbca-BN: First-principles calculations. *Comput. Mater. Sci.* **2014**, *85*, 80–87. [CrossRef]
34. Anderson, O.L. A simplified method for calculating the Debye temperature from elastic constants. *J. Phys. Chem. Solids* **1963**, *24*, 909–917. [CrossRef]
35. Screiber, E.; Anderson, O.L.; Soga, N. *Elastic Constants and Their Measurement*; McGraw-Hill: New York, NY, USA, 1973.
36. Duan, Y.H.; Huang, B.; Sun, Y.; Peng, M.J.; Zhou, S.G. Stability, elastic properties and electronic structures of the stable Zr–Al intermetallic compounds: A first-principles investigation. *J. Alloys Compd.* **2014**, *590*, 50–60. [CrossRef]
37. Hu, W.C.; Liu, Y.; Li, D.J.; Zeng, X.Q.; Xu, C.S. First-principles study of structural and electronic properties of C14-type Laves phase Al_2Zr and Al_2Hf. *Comput. Mater. Sci.* **2014**, *83*, 27–34. [CrossRef]
38. Li, J.; Zhang, M.; Luo, X. Theoretical investigations on phase stability, elastic constants and electronic structures of $D0_{22}$– and $L1_2$-Al_3Ti under high pressure. *J. Alloys Compd.* **2013**, *556*, 214–220.